BENIN JOURNAL OF PHYSICAL SCIENCES
BJPS Vol. 2(2), December, pg. 60-78 (2025)
ISSN 3043-6931(Print)
3043-694X(Online)
www.bjps.org.ng

Well Test Analysis of Horizontal Well in an Anisotropic Reservoir Without Top and Bottom Boundaries

J. E. IGBINEDION*,[1] and E. S. ADEWOLE[2]

[1]*Department of Petroleum Engineering, Federal University of Petroleum Resources Effurun, Delta State, Nigeria*
[2]*Department of Petroleum Engineering, University of Benin, Benin City, Nigeria*

Received: 25/09/2025 ***Accepted:*** 24/11/2025

Abstract

If an oil reservoir has significant height and is bounded laterally by sealing boundaries, optimizing oil production using a horizontal well requires varying the well location along the open vertical axis, especially in highly anisotropic reservoirs. This work analyzes early, transitional, and late-time dimensionless pressure and its derivative responses for a horizontal well in an anisotropic reservoir that is vertically unbounded but laterally sealed. The main objective is to investigate reservoir conditions and well design that prolong oil production despite anisotropy and sealing boundaries. The dimensionless pressure model was developed using source and Green's functions. Late-time responses were quantified, dominant parameters identified, and the onset of transitional and late-time flow was estimated using Odeh and Babu strategies. Wellbore skin and storage effects were not considered. Results show that longer horizontal wells hasten boundary effects, while shorter wells prolong production. Larger reservoir length delays late-time flow due to distant lateral boundaries. Smaller well widths offer larger and longer productivity. Higher anisotropic ratios increase productivity across all flow periods. Dimensionless pressure and its derivative characterize late-time flow, increasing with well length, reservoir dimensions, and permeability. Pressure gradients vary with flow time during the early period, remain constant during the early transient, and increase in late time due to the sealing of boundaries. The onset of boundary effects depends on reservoir anisotropy, well width, and well length. These findings provide guidance for well design and placement to optimize oil production.

Keywords: *Horizontal Well, Dimensionless pressure, Without top and bottom boundaries, Anisotropic Reservoir*

An Official Journal of the Faculty of Physical Sciences, University of Benin, Benin City, Nigeria.

*Corresponding author e-mail: igbinedionjoshua8@gmail.com

1. INTRODUCTION

Rising global hydrocarbon demand and the shift towards complex, unconventional reservoirs have accelerated the adoption of horizontal drilling, which extends reservoir contact, enhances recovery in thin/fractured formations, and mitigates issues such as gas and water coning. This widespread use has reshaped reservoir management and, in particular, Pressure Transient Analysis (PTA). Unlike vertical wells with simpler radial symmetry, horizontal wells exhibit complex, three-dimensional, anisotropy-affected flow that complicates regime identification and parameter estimation. Transient testing (drawdown/buildup) remains central for inferring permeability, skin, boundaries, and drainage geometry, aided by downhole production logging that enables reliable rate control and real-time measurements, making drawdown data increasingly as informative as buildup.

Foundational literature on reservoir system characterization has thoroughly addressed the behavior of flow in horizontal wells; Idudje and Adewole (2020) introduced an improved approach for analyzing pressure drawdown tests of horizontal wells in a completely infinite-acting reservoir system, Wang et al. (2023) developed a detailed pressure transient analysis for multistage fractured horizontal wells, Cui et al. (2023) proposed a semi-analytical model for fractured horizontal wells in shale reservoirs, and Huang et al. (2022) modeled transient flow in fractured horizontal wells considering stress sensitivity. Bourdet et al. (1984) established the groundwork for applying pressure derivatives in well test interpretation. Interpretation relies on analytical and semi-analytical models and non-linear regression to match observed pressure behavior and delineate possible flow regimes. Though their visibility depends on reservoir extent, well length, and vertical/horizontal permeability contrasts. Zhao et al. (2022) demonstrated that horizontal-well testing is still more uncertain than for vertical wells due to multiple overlapping regimes, persistent wellbore storage, and loss of radial symmetry. Agho (2022) analyzed the pressure and pressure derivative behavior of a horizontal well subjected to a single edge and bottom water drive mechanism in an anisotropic reservoir. Olokor and Adewole (2024) extended horizontal-well modeling by developing analytical expressions for transient pressure responses in vertically extensive reservoirs, emphasizing the influence of reservoir anisotropy and boundary configurations on pressure-derivative responses. In addition, Liu et al. (2025) developed a semi-analytical framework for diagnosing transient flow regimes in multi-fractured horizontal wells within deep coalbed methane reservoirs, further demonstrating the continued advancement of pressure-transient modeling for modern horizontal well systems. Gringarten (2008) indicated that most prevailing models assume vertical boundaries, whereas many

real reservoirs are effectively vertically unbounded, risking misinterpretation. Horizontal wells are costlier than vertical wells and exhibit more complex pressure behavior. This study analyzes pressure and pressure derivatives and key characteristics for a horizontal well in a vertically boundless anisotropic reservoir. Its objective, following a similar approach to that previously applied by Orene and Adewole (2020), is to determine early and late-time dimensionless pressure and dimensionless pressure derivatives using dimensionless equations, identify the dimensionless parameters that most strongly influence the responses, and estimate the minimum time for steady-state conditions to occur. It also addresses that gap by developing models and interpretations tailored to horizontally completed wells in vertically open systems to improve characterization and field decisions.

2. MATERIALS AND METHOD

The figure below (Figure 1) depicts the anisotropic, rectangular reservoir model examined in this study. It features a horizontal well with the formation exhibiting directional permeabilities along the x, y, and z axes.

The reservoir is vertically boundless (no boundaries in the z axis) but with a lateral extent (sealing boundaries in the x and y axes). The well is oriented parallel to the reservoir's lateral planes.

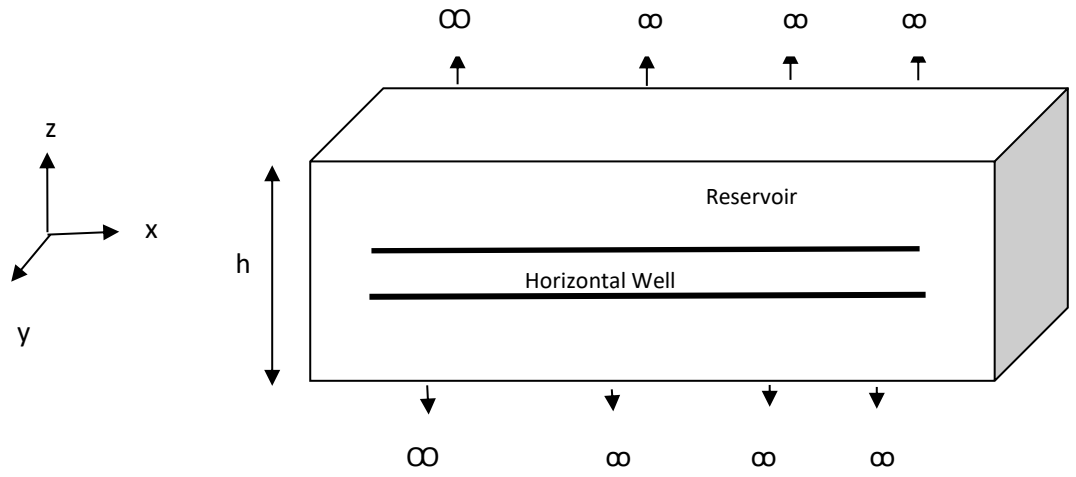

Figure 1: *Horizontal well in a reservoir without top and bottom boundaries but with sealed lateral boundaries.*

2.1 Development of Mathematical Equation

The well is modeled as a line source producing oil at a constant rate q from a reservoir with initial pressure pi, resulting in a drawdown Δp. For this reservoir system, we assume a heterogeneous and anisotropic Formation. Where $k_x \neq k_y \neq k_z$ with lateral flow boundaries. To streamline the mathematics, dimensionless

analysis was used to simplify computations, condense otherwise bulky expressions, and enable clearer graphical interpretation. The dimensionless pressure corresponding to the pressure drop is computed using the appropriate instantaneous-source (Green's) function, following its application developed by Gringarten and Ramey (1973). The general integral solutions for the dimensionless pressure p_D In the context of horizontal wells are often derived from the source and Green's function, given as:

$$p_D = 2\pi h_D \int_0^{tD} s(x_D, y_D, z_D, \tau) d\tau \quad (1)$$

Given that,

$$s(x_D, y_D, z_D, t_D) = s(x_D, t_D).s(y_D, t_D).s(z_D, t_D) \quad (2)$$

2.1.1 Early Radial Flow Model

During this period, the reservoir entirely exhibits infinite-acting behavior because the pressure transient has not yet encountered any boundaries. The corresponding s and Green's functions are selected as described below.

Gringarten and Ramey (1973) established the Green's function for the three horizontal well axes for early flow time as:

X axis

The Green's function of the x-axis is an infinite slab source in an infinite slab reservoir, and at early flow time is:

$$s(x_D, t_D) = ½ \left[\text{erf} \left(\frac{\frac{k}{k_x} + x_D}{2\sqrt{t_D}} \right) + \text{erf} \left(\frac{\frac{k}{k_x} - x_D}{2\sqrt{t_D}} \right) \right] \quad (3)$$

Y axis

The Green's function of the y-axis is an infinite plane source in an infinite slab reservoir, and is given at early flow time:

$$s(y_D, t_D) = \frac{1}{2\sqrt{\pi t_D}} \, exp \left(-\frac{(y_D - y_{wD})^2}{4t_D} \right) \quad (4)$$

Z axis

Lastly, the Green's function for the z-axis is an infinite plane source in an infinite slab reservoir, and is given at early flow time, as:

$$s(z_D, t_D) = \frac{1}{2\sqrt{\pi t_D}} \, exp \left(-\frac{(z_D - z_{wD})^2}{4t_D} \right) \quad (5)$$

According to Equation 1, the dimensionless pressure response of the horizontal well during early-time flow, as established by Gringarten and Ramey (1973) using Newman's product rule, is expressed as:

$$p_D = \frac{h_D}{4}\int_0^{t_D}\left[\left(erf\left(\frac{\frac{k}{k_x}+x_D)}{2\sqrt{\tau}}\right)+erf\left(\frac{\frac{k}{k_x}-x_D}{2\sqrt{\tau}}\right)\right)\frac{1}{\tau}.e^{\left(-\frac{(y_D-y_{wD})^2+(z_D-z_{wD})^2}{4\tau}\right)}\right]d\tau \quad (6)$$

For a fully anisotropic reservoir, Equation 6 becomes:

$$p_D = \frac{h_D}{4}\sqrt{\frac{k}{k_y}}.\sqrt{\frac{k}{k_z}}\int_0^{t_D}\left[\left(erf\left(\frac{\frac{k}{k_x}+x_D)}{2\sqrt{\tau}}\right)+erf\left(\frac{\frac{k}{k_x}-x_D}{2\sqrt{\tau}}\right)\right).\frac{1}{\tau}.e^{\left(-\frac{(y_D-y_{wD})^2+(z_D-z_{wD})^2}{4\tau}\right)}\right]d\tau \quad (7)$$

This can be simply written as:

$$p_D = \frac{h_D}{4}\frac{k}{\sqrt{k_y k_z}}\int_0^{t_D}\left[\left(erf\left(\frac{\frac{k}{k_x}+x_D)}{2\sqrt{\tau}}\right)+erf\left(\frac{\frac{k}{k_x}-x_D}{2\sqrt{\tau}}\right)\right).\frac{1}{\tau}.e^{\left(-\frac{(y_D-y_{wD})^2+(z_D-z_{wD})^2}{4\tau}\right)}\right]d\tau \quad (8)$$

The dimensionless pressure derivative is given as:

$$p'_D = t_D\frac{\partial p_D}{\partial t_D} \quad (9)$$

By substitution, we have;

$$p'_D = \frac{h_D}{4}\frac{k}{\sqrt{k_y k_z}}\left[\left(erf\left(\frac{\frac{k}{k_x}+x_D)}{2\sqrt{\tau}}\right)+erf\left(\frac{\frac{k}{k_x}-x_D}{2\sqrt{\tau}}\right)\right).e^{\left(-\frac{(y_D-y_{wD})^2+(z_D-z_{wD})^2}{4t_D}\right)}\right] \quad (10)$$

2.1.2 Transition Time Flow Period

According to Gringarten and Ramey (1973), during the transition time flow period, the external boundaries of the reservoir along the x and y axes might be felt one at a time. If the x-axis boundary is felt, then the source function is that of an infinite slab source in an infinite slab reservoir with both ends sealed, and it's given as:

$$s(x_D, t_D) = \frac{1}{x_{eD}}\left[1+\frac{4x_{eD}}{\pi x_f}\sum_{=1}^{\infty}\exp\left(-\frac{n^2\pi^2 t_D}{{x_{eD}}^2}\right)sin\frac{n\pi x_f}{2x_{eD}}cos\frac{n\pi x_{wD}}{x_{eD}}cos\frac{n\pi x_D}{x_{eD}}\right] \quad (11)$$

Then the Green's functions for the y and z axes remain as described in Equations 4 and 5, respectively.

Therefore, applying the Newmann product rule as established by Gringarten and Ramey (1973), the transitional flow model, when only the x-axis is felt, is given as:

$$p_D = \frac{h_D}{2x_{eD}}\frac{k}{\sqrt{k_y k_z}}\int_0^{t_D}\left[\left(1 + \frac{4x_{eD}}{\pi}\sum_{n=1}^{\infty}\frac{1}{n}e^{\left(-\frac{n^2\pi^2\tau}{x_{eD}{}^2}\right)}sin\left(\frac{n\pi}{x_{eD}}\right)cos\left(\frac{n\pi x_{wD}}{x_{eD}}\right)cos\left(\frac{n\pi x_D}{x_{eD}}\right)\right)\left(e^{-\frac{(y_D-y_{wD})^2+(z_D-z_{wD})^2}{4\tau}}\right)\right]\frac{d\tau}{\tau} \quad (12)$$

And the dimensionless pressure derivative is given as:

$$p'_D = \frac{h_D}{2x_{eD}}\frac{k}{\sqrt{k_y k_z}}\left\{\left[\left(1 + \frac{4x_{eD}}{\pi}\sum_{n=1}^{\infty}\frac{1}{n}e^{\left(-\frac{n^2\pi^2t_D}{x_{eD}{}^2}\right)}sin\left(\frac{n\pi}{x_{eD}}\right)cos\left(\frac{n\pi x_{wD}}{x_{eD}}\right)cos\left(\frac{n\pi x_D}{x_{eD}}\right)\right)\left(e^{-\frac{(y_D-y_{wD})^2+(z_D-z_{wD})^2}{4t_D}}\right)\right]\right\} \quad (13)$$

If the y-axis boundary is felt first, then the y-axis source function is an infinite point source in an infinite slab reservoir with both boundaries sealing. This is given in Equation (14).

$$s(y_D, t_D) = \left[1 + 2\sum_{n=1}^{\infty}e^{-\frac{n^2\pi^2\tau^2}{y_{eD}{}^2}}cos\left(\frac{n\pi y_{wD}}{y_{eD}}\right)cos\left(\frac{n\pi y_D}{y_{eD}}\right)\right] \quad (14)$$

Now applying Equations (1) and (9), the transitional p_D and p'_D derived are given, respectively, as:

$$p_D = \frac{\sqrt{\pi}h_D}{2y_{eD}}\sqrt{\frac{k}{k_Z}}\int_0^{t_D}\left\{\left[erf\left(\frac{\sqrt{\frac{k}{k_x}}+(x_D-x_{wD})}{2\sqrt{\tau}}\right)+erf\left(\frac{\sqrt{\frac{k}{k_x}}-(x_D-x_{wD})}{2\sqrt{\tau}}\right)\right]\left[1 + 2\sum_{n=1}^{\infty}e^{-\frac{n^2\pi^2\tau^2}{y_{eD}{}^2}}cos\left(\frac{n\pi y_{wD}}{y_{eD}}\right)cos\left(\frac{n\pi y_D}{y_{eD}}\right)\right]\left[e^{-\frac{(z_D-z_{wD})^2}{4t_D{}^2}}\right]\right\} \quad (15)$$

and

$$p'_D = \frac{\sqrt{\pi}h_D}{2y_{eD}}\sqrt{\frac{k}{k_Z}}\left\{\left[erf\left(\frac{\sqrt{\frac{k}{k_x}}+(x_D-x_{wD})}{2\sqrt{\tau}}\right)+erf\left(\frac{\sqrt{\frac{k}{k_x}}-(x_D-x_{wD})}{2\sqrt{\tau}}\right)\right]\left[1 + 2\sum_{n=1}^{\infty}e^{-\frac{n^2\pi^2\tau^2}{y_{eD}{}^2}}cos\left(\frac{n\pi y_{wD}}{y_{eD}}\right)cos\left(\frac{n\pi y_D}{y_{eD}}\right)\right]\left[e^{-\frac{(z_D-z_D{}')^2}{4t_D{}^2}}\right]\right\}\sqrt{t_D} \quad (16)$$

2.1.3 Late Time Flow Period

In this flow period, the x and y boundaries are felt together while the z boundary remains infinite-acting. All the external boundaries along both the x and y axes are now felt. Therefore, the dimensionless pressure and its derivative are derived respectively as:

$$p_D = \frac{\sqrt{\pi} h_D}{x_{eD} y_{eD}} \sqrt{\frac{k}{k_Z}} \int_0^{t_D} \left[\left(1 + \frac{2x_{eD}}{\pi} \sum_{n=1}^{\infty} \frac{1}{n} e^{\left(-\frac{n^2\pi^2\tau}{x_{eD}{}^2}\right)} sin\left(\frac{n\pi}{x_{eD}}\right) cos\left(\frac{n\pi x_{wD}}{x_{eD}}\right) cos\left(\frac{n\pi x_D}{x_{eD}}\right) \right) \left(1 + 2 \sum_{n=1}^{\infty} e^{-\frac{n^2\pi^2\tau}{y_{eD}{}^2}} cos\left(\frac{n\pi y_{wD}}{y_{eD}}\right) cos\left(\frac{n\pi y_D}{y_{eD}}\right) \right) \left(e^{-\frac{(z_D - z_{wD})^2}{4\tau}} \right) \right] \frac{d\tau}{\sqrt{\tau}} \quad (17)$$

and

$$p'_D = \frac{\sqrt{\pi} h_D}{x_{eD} y_{eD}} \sqrt{\frac{k}{k_Z}} \left\{ \left[\left(1 + \frac{2x_{eD}}{\pi} \sum_{n=1}^{\infty} \frac{1}{n} e^{\left(-\frac{n^2\pi^2\tau}{x_{eD}{}^2}\right)} sin\left(\frac{n\pi}{x_{eD}}\right) cos\left(\frac{n\pi x_{wD}}{x_{eD}}\right) cos\left(\frac{n\pi x_D}{x_{eD}}\right) \right) \left(1 + 2 \sum_{n=1}^{\infty} e^{\left(-\frac{n^2\pi^2\tau}{y_{eD}{}^2}\right)} cos\left(\frac{n\pi y_{wD}}{y_{eD}}\right) cos\left(\frac{n\pi y_D}{y_{eD}}\right) \right) \left(e^{-\frac{(z_D - z_{wD})^2}{4\tau}} \right) \right] \right\} \sqrt{t_D} \quad (18)$$

Odeh and Babu (1989) established strategies to delineate the flow periods. The strategies utilize reservoir fluid and wellbore properties to compute dimensionless pressures and their derivatives from one flow period starting from a dimensionless time equal to zero. The strategies effectively determine the integration intervals in all the dimensionless pressure and dimensionless pressure derivative expressions derived above. The strategies were employed in this study to compute the intervals of integration in all the integrals stated above.

3. RESULT AND DISCUSSION

Table 1: *Reservoir system parameters*

Par.	k_x (md)	k_y (md)	k_z (md)	k (md)	h (ft)	L (ft)	r_w (ft)	$\emptyset$	x_e (ft)	y_e (ft)	x (ft)	y (ft)	z (ft)	x_w (ft)	y_w (ft)	z_w (ft)
Value	20	60	10	50	200	100	0.5	0.70	2300	2000	2	2	2	5	5	5

The effect of well length was studied by keeping the rest of the parameters constant while varying the dimensionless well length between 0.45, 0.90, 1.35, 1.80,

and 2.25. The equivalent dimensionless parameters at different well lengths required for the computations are contained in Table 2

Table 2: *Equivalent dimensionless parameters*

$L(ft)$	L_D	x_D	x_{wD}	x_{eD}	r_{wD}	y_D	y_{wD}	y_{eD}	z_D	z_{wD}	h_D
400	0.45	0.016	0.040	12.88	0.0023	0.009	0.015	9.10	0.022	0.037	2.24
800	0.90	0.008	0.020	6.44	0.0011	0.005	0.011	4.55	0.011	0.028	1.12
1200	1.35	0.005	0.013	4.29	0.0008	0.003	0.008	3.03	0.007	0.019	0.75
1600	1.80	0.004	0.010	3.22	0.0006	0.002	0.006	2.28	0.006	0.014	0.56
2000	2.25	0.003	0.008	2.58	0.0005	0.002	0.005	1.82	0.004	0.011	0.45

Table 3: *Results of p_D and p'_D for L_D = 0.45, 0.90, 1.35, 1.80, and 2.25*

t_D	L=400ft ($L_D = 0.45$)		L=800ft ($L_D = 0.90$)		L=1200ft ($L_D = 1.35$)		L=1600ft ($L_D = 1.80$)		L=2000ft ($L_D = 2.25$)	
	p_D	p'_D	p_D	p'_D	p_D	p'_D	p_D	p'_D	p_D	p'_D
0.000001	0.2221	0.971058	0.2175	0.501504	0.209	0.323365	0.2082	0.265779	0.194	0.206983
0.00001	0.7286	1.105612	0.6831	0.524584	0.5515	0.371872	0.4794	0.274704	0.4171	0.212016
0.0001	1.7345	1.155053	1.205	0.529859	0.901	0.373458	0.742	0.275093	0.6272	0.212165
0.001	2.7908	1.160502	1.7353	0.530486	2.5283	1.102051	2.8898	0.883723	2.7219	0.716294
0.01	12.8156	3.625905	7.3788	1.770835	5.6514	1.208426	4.7846	0.910085	4.5637	0.724593
0.1	21.6719	3.60921	10.9583	1.776156	7.9819	1.190995	6.5033	0.895495	6.2293	0.712574
1	27.3485	2.467307	13.7448	1.207615	9.8404	0.810249	7.8901	0.611264	7.563	0.485743
10	73.2167	2.733616	37.0268	1.388651	26.7147	1.17629	21.671	1.229809	19.3367	1.354939
100	76.7432	2.803908	40.3566	2.234989	30.8843	2.810807	26.8193	3.443203	25.5684	4.140517
1000	81.5491	3.746117	47.9275	5.531121	41.6395	7.786404	40.6881	10.02101	42.7569	12.4048
10000	93.4233	8.928515	69.6356	15.89592	73.7352	23.43233	82.7694	30.70514	95.3917	38.39212
100000	127.6910	25.30758	136.1305	48.65404	173.4377	72.88157	214.2277	96.07771	260.3184	120.5255
1000000	232.7849	77.09983	344.2781	152.23860	486.9686	229.24510	628.37040	302.79240	780.4068	380.23961

Figure 2 is a log-log plot of p_D and p'_D against t_D for L_D = 0.45, 0.90, 1.35, 1.80, and 2.25.

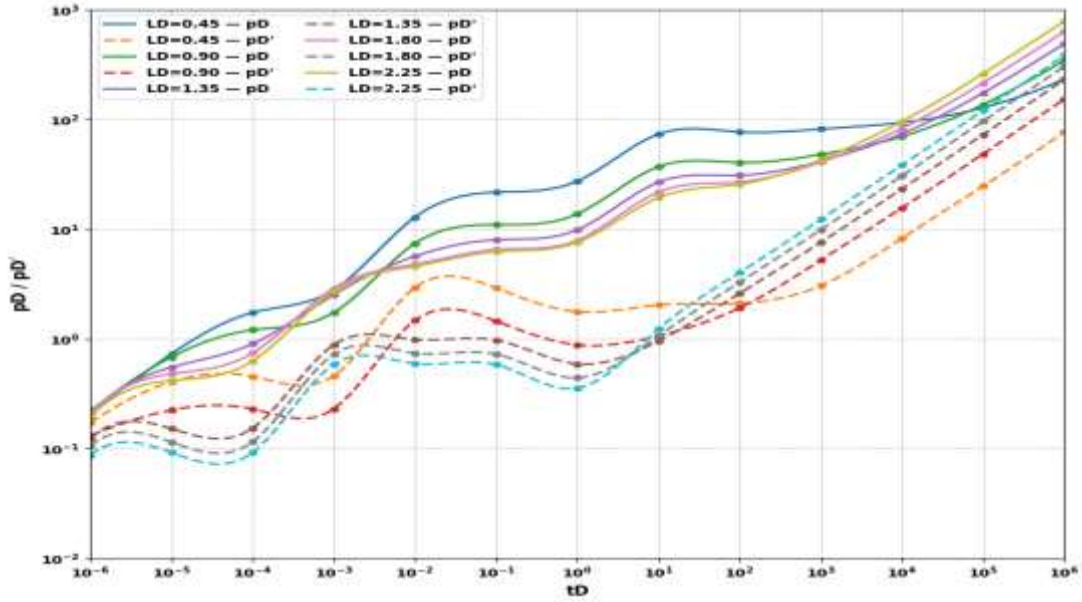

Figure 2: *Log-log plot showing the effect of well length on p_D and p'_D*

Table 4 and Figure 3 show results for different reservoir lengths while retaining the values of reservoir system parameters stated in Table 1

Table 4: *Results of p_D and p'_D for x_{eD} = 158, 316, 474, 632, and 790*

t_D	xe=5000ft (x_{eD} = 158)		xe=1000ft (x_{eD} = 316)		xe=15000ft (x_{eD} = 474)		xe=20000ft (x_{eD} = 632)		xe=25000ft (x_{eD} = 790)	
	p_D	p'_D	p_D	p'_D	p_D	p'_D	p_D	p'_D	p_D	p'_D
0.000001	0	0	0	0	0	0	0	0	0	0
0.00001	0.2192	0.612344	0.2192	0.612344	0.2192	0.612344	0.2192	0.612344	0.2192	0.612344
0.0001	5.625	3.78876	5.625	3.78876	5.625	3.78876	5.625	3.78876	5.625	3.788760
0.001	15.5066	4.546186	15.5066	4.546186	15.5066	4.546186	15.5066	4.546186	15.5066	4.546186
0.01	26.1047	4.6298	26.1047	4.6298	26.1047	4.6298	26.1047	4.6298	26.1047	4.629800
0.1	47.5255	11.99138	48.7306	12.781701	48.9716	12.93818	47.6484	12.04617	46.2303	11.085125
1	99.278	9.563205	102.3409	9.563205	102.9078	9.563019	98.2747	9.549743	92.782	9.477786
10	233.4519	10.77419	242.0609	10.774189	243.6388	10.77419	230.1808	10.77419	214.0327	10.774189
100	253.178	6.306899	261.7869	6.306899	263.3648	6.306899	249.9071	6.306899	233.7587	6.306899
1000	266.2689	5.353358	274.8778	5.353358	276.4557	5.353358	262.9978	5.353358	246.8496	5.353358
10000	277.1771	5.25031	285.7831	5.241809	287.361	5.241805	273.9031	5.241805	257.7549	5.241805
100000	291.9656	6.649608	299.3282	5.644499	300.6903	5.325902	287.197	5.226793	271.0447	5.208124
1000000	311.2251	10.87166	314.2989	7.755423	314.2349	6.716677	300.053	6.197304	283.5275	5.885681

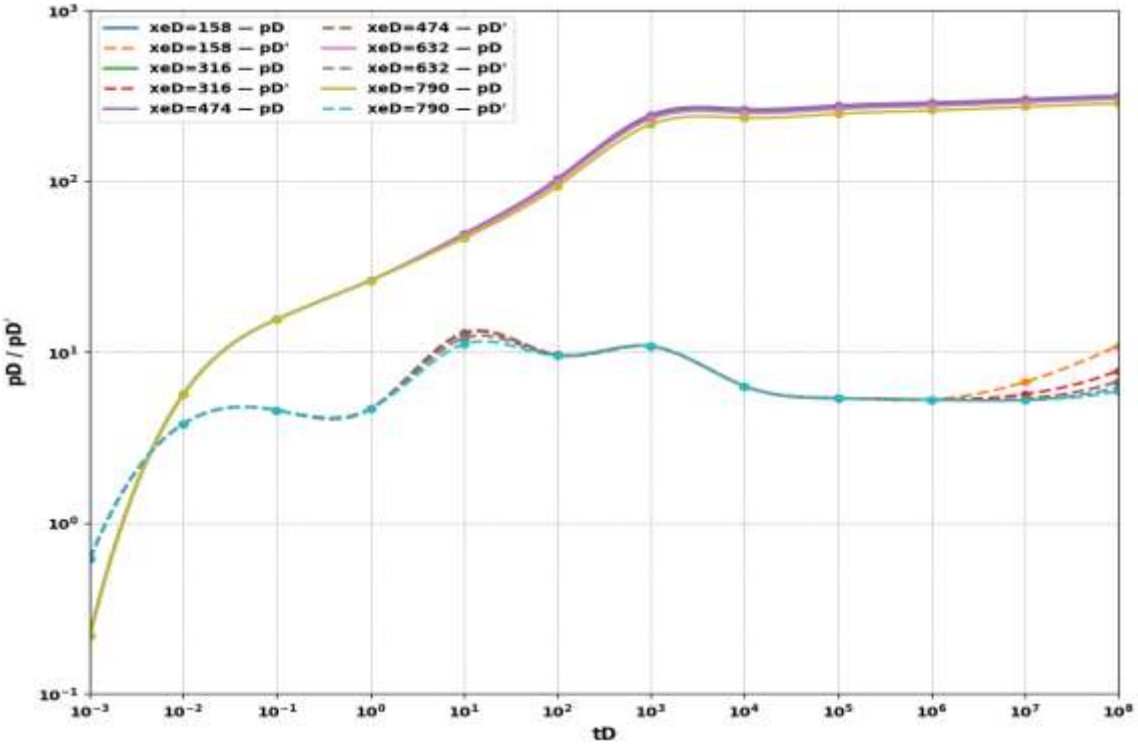

Figure 3: *Log-log plot showing the effect of reservoir length on p_D and p'_D*

Table 5 and Figure 4 show the effect of reservoir width on dimensionless pressure p_D and its derivative p'_D

Table 5: *Results of p_D and p'_D for y_{eD} = 91, 182, 273, 364, and 455*

t_D	ye=5000ft (y_{eD} = 91)		ye=1000ft (y_{eD} = 182)		ye=15000ft (y_{eD} = 273)		ye=20000ft (y_{eD} = 364)		ye=25000ft (y_{eD} = 455)	
	p_D	p'_D	p_D	p'_D	p_D	p'_D	p_D	p'_D	p_D	p'_D
0.0001	0	0	0	0	0	0	0	0	0	0
0.001	0.2175	0.612344	0.2175	0.612344	0.2175	0.612344	0.2175	0.612344	0.2175	0.612344
0.01	5.625	3.78876	5.625	3.78876	5.625	3.78876	5.625	3.78876	5.625	3.78876
0.1	15.5066	4.546186	15.5066	4.546186	15.5066	4.546186	15.5066	4.546186	15.5066	4.546186
1	26.1047	4.6298	26.1047	4.6298	26.1047	4.6298	26.1047	4.6298	26.1047	4.6298
10	47.6153	12.05665	47.6153	12.05665	47.6153	12.05665	47.6153	12.05665	47.6153	12.05665
100	99.4588	9.563205	99.4588	9.563205	99.4588	9.563205	99.4588	9.563205	99.4588	9.563205
1000	233.0611	10.77419	224.1367	10.79419	214.7929	10.77419	206.8091	10.77419	200.0652	10.77419
10000	250.5505	7.415494	241.6262	7.415494	232.2823	7.415494	224.2986	7.415494	217.5546	7.415494
100000	265.7651	5.165816	256.8407	5.165639	247.4969	5.165639	239.5131	5.165639	232.7692	5.165639
1000000	277.2831	5.340434	268.1958	5.099496	258.8471	5.07977	250.8633	5.079452	244.1194	5.079451
10000000	290.8796	6.461619	280.6401	5.61327	270.9541	5.330489	262.846	5.189589	256.0543	5.110032
100000000	309.1889	10.13045	295.2805	7.447683	284.3716	6.553429	275.6521	6.106302	268.4945	5.838026

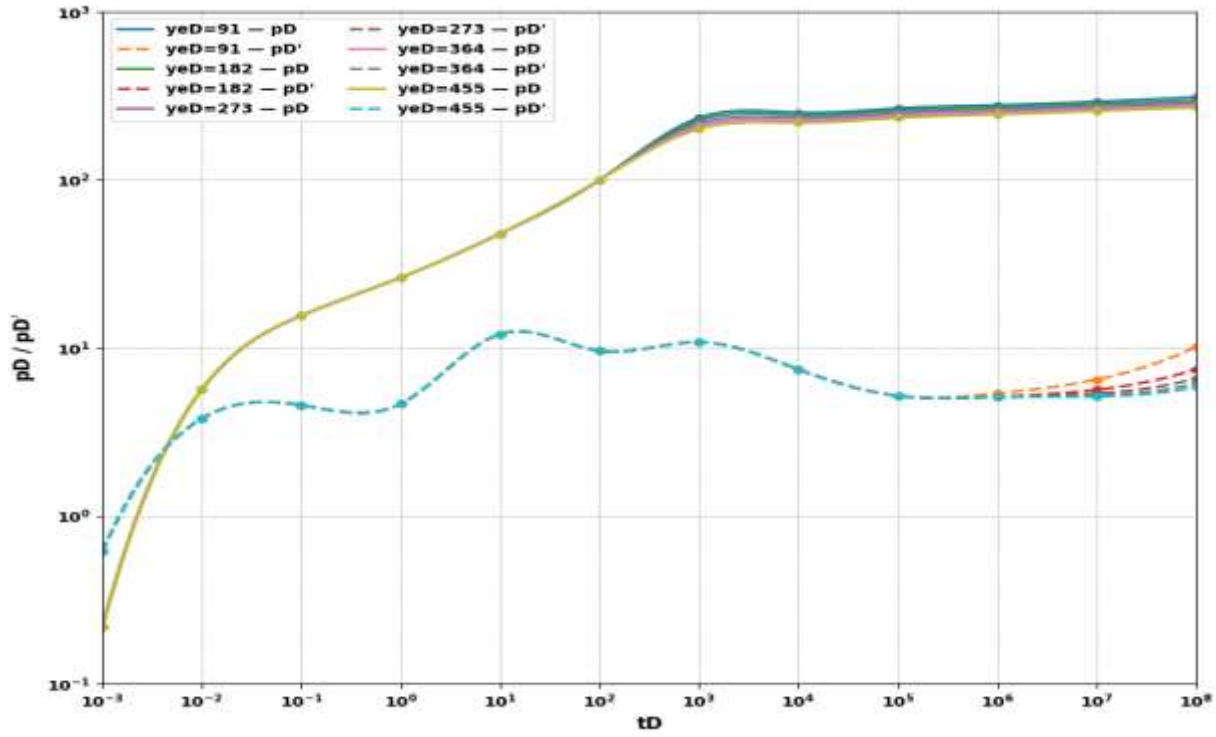

Figure 4: *Log-log plot showing the effect of reservoir width on p_D and p'_D*

Table 6 and Figure 5 show the effect of parallel reservoir permeability k_x on dimensionless pressure p_D and its derivative p'_D

Table 6: *Results of p_D and p'_D for k_x = 10, 12, 20, 25, and 30*

t_D	$(k_x = 10)$		$(k_x = 15)$		$(k_x = 20)$		$(k_x = 25)$		$(k_x = 30)$	
	p_D	p'_D	p_D	p'_D	p_D	p'_D	p_D	p'_D	p_D	p'_D
0.000001	0	0	0	0	0	0	0	0	0	0
0.00001	0.2192	0.612344	0.2192	0.612344	0.2192	0.612344	0.2192	0.612344	0.2192	0.612344
0.0001	5.625	3.78876	5.625	3.78876	5.625	3.78876	5.625	3.78876	5.625	3.78876
0.001	26.3656	11.96769	26.3665	11.96769	26.3664	11.96769	26.3665	11.96769	26.3665	11.96769
0.01	161.3845	26.78311	173.7336	23.38728	177.0158	22.2503	178.5075	21.68535	179.3781	21.34704
0.1	214.9677	9.951628	215.2137	9.901812	215.365	9.904636	215.3944	9.863369	215.414	9.853952
1	233.0398	6.288727	233.1873	6.289976	233.2932	6.302934	233.3018	6.333715	233.3169	6.382375
10	246.4072	5.866823	246.8569	6.142648	247.276	6.375442	247.594	6.58061	247.9084	6.765698
100	261.8264	7.910241	263.3407	8.645476	264.6575	9.265607	265.7668	9.812161	266.7951	10.30523
1000	286.0864	14.37555	290.6526	16.56398	294.5434	18.40974	297.9213	20.03651	300.9962	21.50409
10000	338.3056	34.8204	352.2081	41.6043	363.9732	47.32586	374.2911	52.36858	383.6271	56.91786
100000	478.9394	99.47264	522.0518	120.7887	558.4523	138.7666	590.4828	154.6115	619.4066	168.906
1000000	899.1654	303.9209	1034.333	371.1917	1147.372	427.9276	1248.83	477.932	1339.485	523.0436

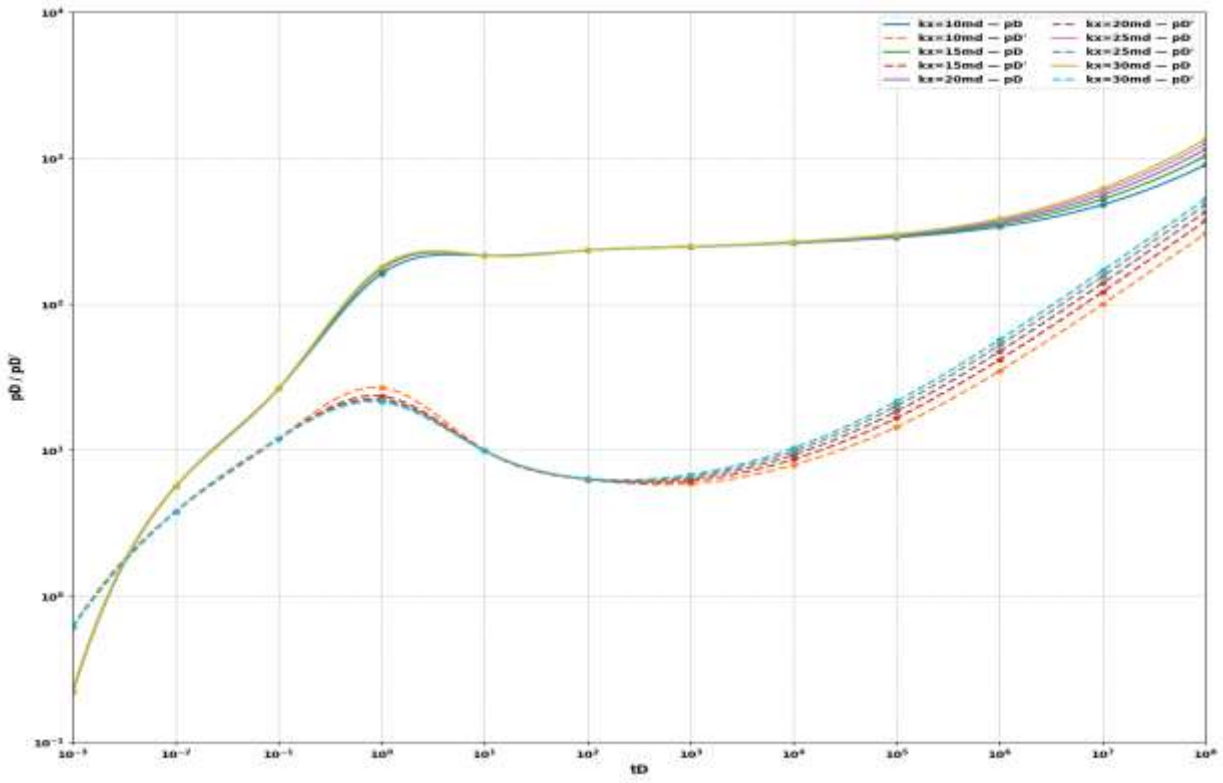

Figure 5: *Log-log plot showing the effect of k_x on p_D and p'_D*

Table 7 and Figure 6 show the effect of horizontal reservoir permeability k_y on dimensionless pressure p_D and its derivative p'_D.

Table 7: *Results of p_D and p'_D for k_y = 50, 70, 90, 110, and 130*

t_D	$(k_y = 50)$		$(k_y = 70)$		$(k_y = 90)$		$(k_y = 110)$		$(k_y = 130)$	
	p_D	p'_D	p_D	p'_D	p_D	p'_D	p_D	p'_D	p_D	p'_D
0.000001	0.0559	0.169383	0.0472	0.143155	0.2628	0.440658	0.2377	0.39859	0.2186	0.36665
0.00001	1.8118	1.283264	1.5312	1.084556	2.1836	1.083844	1.9751	0.980373	1.8168	0.901812
0.0001	5.2059	1.571306	4.3998	1.327996	4.8368	1.185914	4.375	1.072699	4.0244	0.98674
0.001	12.7735	4.202148	10.8548	3.563025	10.5586	3.146807	9.5885	2.853553	8.8201	2.624888
0.01	30.7603	3.312563	26.069	2.799669	23.981	2.459237	21.7371	2.233534	19.9953	2.054553
0.1	162.3973	6.681128	158.0948	6.345191	156.1999	6.128713	154.1361	5.974404	152.3199	5.857509
1	173.8957	3.37645	169.1489	3.382541	167.0938	3.453684	165.0181	3.550487	163.2806	3.660523
10	181.5468	3.263471	176.8674	3.299018	175.0042	3.385814	173.1723	3.493766	171.7052	3.612602
100	190.8051	5.509654	186.536	5.961613	185.1552	6.407053	183.8241	6.835802	182.8631	7.250304
1000	211.2988	13.85611	209.5017	15.83838	210.381	17.60352	211.1421	19.21361	212.1546	20.71748
10000	267.8841	40.24846	275.1765	47.06974	283.2644	53.00788	291.9844	58.35349	299.6809	63.30207
100000	438.6037	123.7079	475.9121	145.8314	510.7711	164.9657	542.0879	182.124	571.3650	195.9656
1000000	970.248	387.6298	1103.748	458.143	1221.687	519.0072	1327.443	573.5204	1425.4090	623.8089

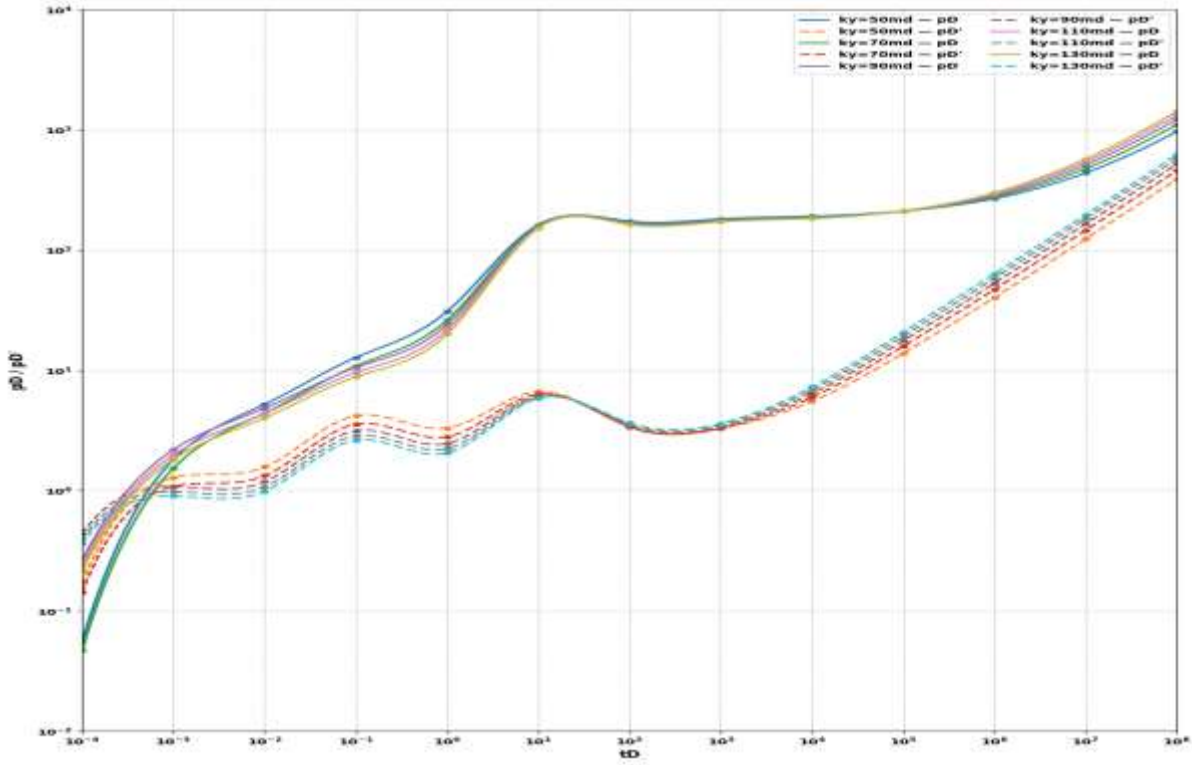

Figure 6: *Log-log plot showing the effect of k_y on p_D and p'_D*

Table 8 and Figure 7 show the effect of vertical reservoir permeability k_z on dimensionless pressure p_D and its derivative p'_D

Table 8: *Results of p_D and p'_D for k_z = 8, 12, 16, 20, and 24*

t_D	$(k_z = 8)$		$(k_z = 12)$		$(k_z = 16)$		$(k_z = 20)$		$(k_z = 24)$	
	p_D	p'_D	p_D	p'_D	p_D	p'_D	p_D	p'_D	p_D	p'_D
0.000001	0.0692	0.046596	0.0463	0.031185	0.0347	0.023367	0.0277	0.018652	0.0231	0.01555
0.00001	0.1907	0.155911	0.1804	0.117078	0.1888	0.11991	0.1714	0.10308	0.1563	0.090251
0.0001	1.2236	0.250159	0.8476	0.221636	0.6428	0.166315	0.5161	0.132219	0.4374	0.111044
0.001	2.0216	0.24611	1.3746	0.2183	1.0354	0.163658	0.827	0.130014	0.6977	0.109113
0.01	2.6495	0.161688	1.7942	0.135005	1.3497	0.101209	1.0765	0.080452	0.907	0.06746
0.1	4.7096	0.162769	3.1893	0.108963	2.3997	0.081685	1.9139	0.064772	1.6144	0.05444
1	4.9938	0.087184	3.3795	0.058363	2.5423	0.043739	2.0275	0.034844	1.7095	0.029131
10	5.1681	0.069014	3.4961	0.046191	2.6298	0.034617	2.0971	0.027604	1.7676	0.023046
100	5.3323	0.077581	3.606	0.051928	2.712	0.038917	2.1628	0.031017	1.8225	0.026315
1000	5.5447	0.113666	3.7481	0.076087	2.8186	0.057034	2.2477	0.045395	1.8935	0.038398
10000	5.9131	0.227771	3.9949	0.152484	3.0035	0.114319	2.3947	0.090859	2.0166	0.076608
100000	6.7751	0.5886	4.5719	0.394068	3.4362	0.295472	2.7382	0.234631	2.3052	0.197436
1000000	9.1973	1.72964	6.1936	1.158026	4.6522	0.868327	3.7037	0.689275	3.1161	0.579529

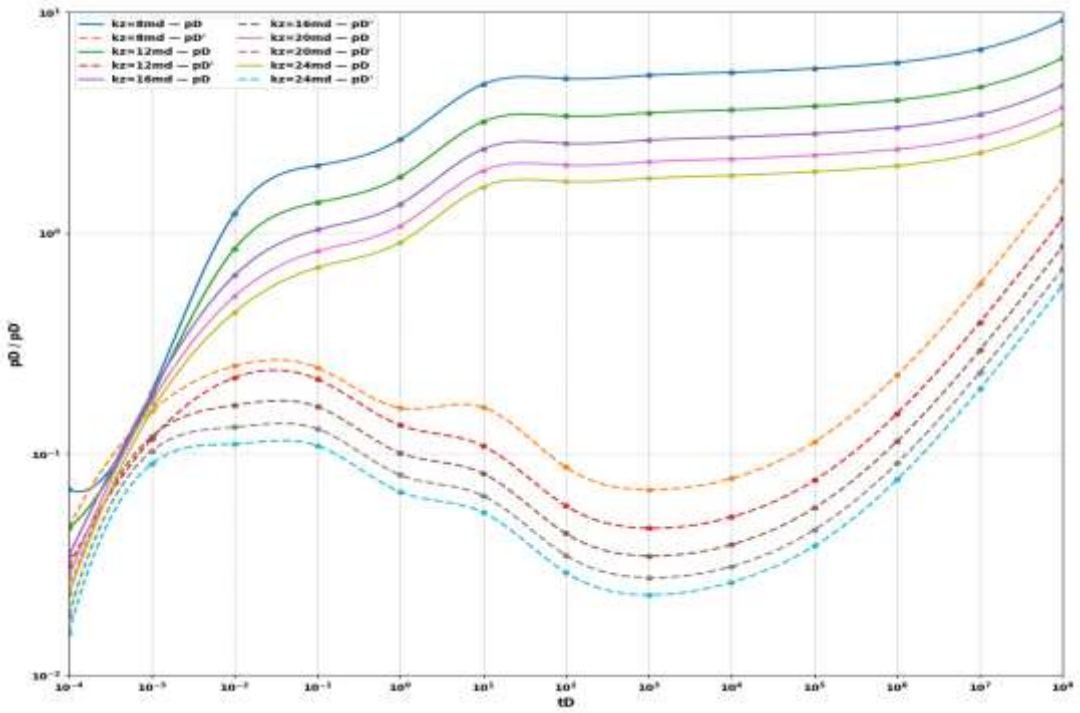

Figure 7: *Log-log plot showing the effect of k_z on p_D and p'_D*

Table 9 and Figure 8 show the effect of the vertical anisotropic ratio $\frac{k}{k_z}$ on dimensionless pressure p_D and its derivative p'_D.

Table 9: *Results of p_D and p'_D for $\frac{k}{k_z}$ = 1, 2, 3, 4, and 5*

t_D	$(\frac{k}{k_z} = 1)$		$(\frac{k}{k_z} = 2)$		$(\frac{k}{k_z} = 3)$		$(\frac{k}{k_z} = 4)$		$(\frac{k}{k_z} = 5)$	
	p_D	p'_D	p_D	p'_D	p_D	p'_D	p_D	p'_D	p_D	p'_D
0.0001	10.99273	33.330161	2.1592	6.546662	3.4002	10.298884	4.2280	12.8193	5.5865	16.9383
0.001	356.5120	252.513000	70.0256	49.598237	110.2218	78.032646	137.1200	97.1204	181.1784	128.3264
0.01	1024.3877	309.192090	201.2088	60.731062	316.6619	95.607093	393.9953	118.9200	520.5910	157.1306
0.1	1746.1649	315.517053	342.9792	61.973402	539.6953	97.557493	671.6019	121.3527	887.3962	160.3449
1	2473.6662	316.156623	485.8739	62.099026	764.5544	97.755218	951.4101	121.5987	1257.1104	160.6699
10	3388.6143	424.071109	906.2981	78.711755	1308.5290	126.27834	1548.6817	175.4884	1809.5434	249.8442
100	4159.2837	316.289138	1140.2046	62.239093	1684.3751	97.996951	2066.7171	121.8871	2622.5785	161.0383
1000	4895.6303	316.229548	1299.7671	62.116699	1934.7424	97.812274	2380.3967	121.6335	3035.0023	160.7154
10000	5626.6617	316.227875	1448.5719	62.113231	2168.7802	97.807720	2672.0350	121.6265	3419.5308	160.7067
100000	6358.5761	316.227789	1599.1389	62.113046	2405.4556	97.807638	2967.1828	121.6262	3808.4369	160.7062
1000000	7095.5854	316.227772	1759.8957	62.113012	2657.4145	97.807612	3282.7089	121.6261	4222.8147	160.7061
10000000	7848.7079	316.227768	1952.8798	62.113003	2957.7118	97.807604	3662.6879	121.6261	4717.7562	160.7061
100000000	8652.7852	316.227767	2247.7760	62.113001	3410.8689	97.807601	4246.4860	121.6261	5467.4638	160.7061

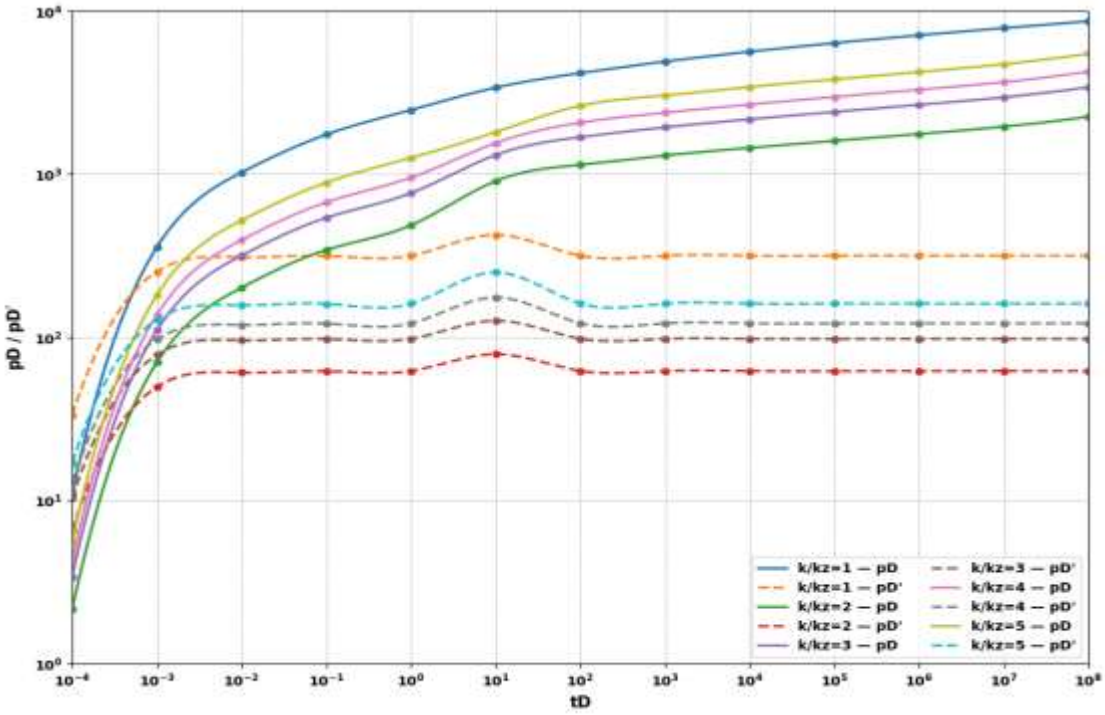

Figure 8: *Log-log plot showing the effect of* $\frac{k}{k_z}$ *on* p_D *and* p'_D

Table 10 and Figure 9 show the effect of the horizontal anisotropic ratio $\frac{k}{k_y}$ on dimensionless pressure p_D and its derivative p'_D.

Table 10: *Results of* p_D *and* p'_D *for* $\frac{k}{k_y}$ *= 3, 5, 7, 9, and 11*

t_D	$(\frac{k}{k_y} = 3)$		$(\frac{k}{k_y} = 5)$		$(\frac{k}{k_y} = 7)$		$(\frac{k}{k_y} = 9)$		$(\frac{k}{k_y} = 11)$	
	p_D	p'_D	p_D	p'_D	p_D	p'_D	p_D	p'_D	p_D	p'_D
0.0001	0	0	0	0	0	0	0	0	0	0
0.001	0.00153	0.0124633	0.00001	0.0001228	0	0	0	0	0	0
0.01	6.13163	8.3106097	3.44541	6.5892912	1.98021	4.8243784	1.03057	3.1247026	0.61062	2.1536724
0.1	36.31012	15.923293	36.50848	19.578769	35.63023	22.0802138	33.423	23.673094	32.07405	24.963742
1	94.78756	33.958293	99.89394	39.255782	103.2661	42.2892881	104.5519	44.079504	106.5424	45.255058
10	163.3138	18.188287	183.3381	23.24778	197.9131	27.3581099	208.0837	30.905563	217.43	34.071843
100	213.3371	17.137144	247.0125	22.122084	272.6372	26.17342	292.321	29.6758	310.1334	32.805939
1000	255.7448	17.116897	301.661	22.097689	337.2333	26.1461999	365.5165	29.646828	391.0134	32.775639
10000	296.2107	17.116366	353.8701	22.097108	398.9877	26.145637	435.5244	29.646349	468.3982	32.775256
100000	336.4877	17.116333	405.8413	22.097089	460.4644	26.1456269	505.2204	29.646353	545.4405	32.775274
1000000	376.8144	17.11633	457.8374	22.097087	521.9552	26.145626	574.9249	29.646353	622.4882	32.775276
10000000	417.432	17.11633	510.0523	22.097087	583.624	26.1456259	644.7799	29.646353	699.6658	32.775277
100000000	458.9799	17.11633	562.9878	22.097087	645.9019	26.145628	715.1719	29.646353	777.3293	32.775277

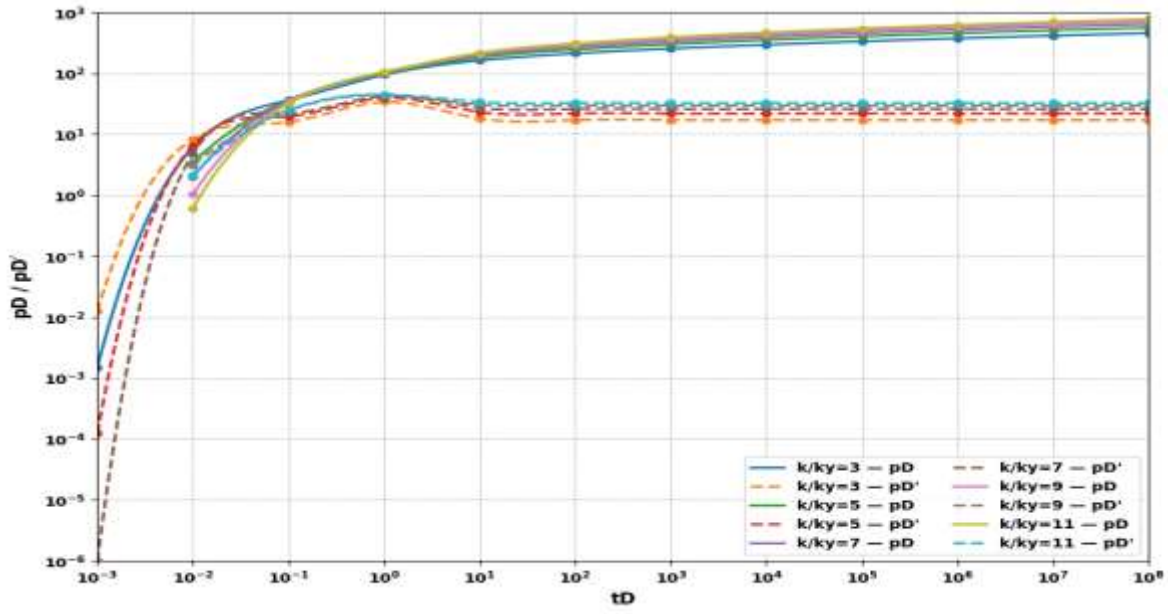

Figure 9: *Log-log plot showing the effect of* $\frac{k}{k_y}$ *on* p_D *and* p'_D

Dimensionless pressure and its derivative were computed across a range of reservoir and well parameters. The interference of the boundless reservoir top was mostly felt during the late-time flow periods. As summarized in Table 3 and Figure 2, increasing well length reduces both dimensionless pressure and its derivative in an anisotropic reservoir. Longer wells encounter the sealing boundaries sooner; consequently, in a vertically unbounded reservoir, longer well lengths will require external pressure support earlier because the lateral boundaries are sealing. Consequently, in an anisotropic reservoir with boundless top and bottom, longer laterals tend to accelerate the encroachment of the sealing boundary effect into the wellbore, whereas shorter laterals prolong productive performance. Results in Table 4 and Figure 3 show that the length of the reservoir does not affect the dimensionless pressure and its derivative at early time since all the boundaries are infinite-acting; but at transitional and late flow periods, the dimensionless pressure and its derivative reduce with increasing reservoir length to an extent and a decrease in the dimensionless pressure and its derivative is experienced due to the presence of a sealing boundary. Table 5 and Figure 4 show that the dimensionless pressure and its derivative are unaffected by reservoir width at early times but decrease with increasing reservoir width during late flow periods due to the influence of the sealing reservoir boundaries. This explains the fact that reservoirs in the study scenario with larger reservoir width will improve the oil production; the same case for a reservoir with a longer length. Tables 4 and 5, together with Figures 3 and 4, show that the reservoir width and length have the same impact on the pressure and the oil production in a vertically boundless reservoir. Table 6 and Figure 5 show that the dimensionless pressure and its derivative increase with the permeability of the reservoir parallel to the well. Table

7 and Figure 6 also show that the dimensionless pressure and its derivative increase with the horizontal permeability. Table 8 and Figure 7 show that the dimensionless pressure and its derivative decrease with the vertical permeability, and this can be attributed to the fact that the vertical boundary is never felt in this case study. Table 9 and Figure 8 show that the dimensionless pressure and its derivative increase with increasing horizontal anisotropic ratio. Table 10 and Figure 9 show that the dimensionless pressure and its derivative increase with increasing vertical anisotropic ratio. Findings from Tables 6 to 10, as well as Figures 5 to 9, prove that permeability, which is a good metric to measure reservoir quality, generally improves the oil production in the reservoir.

4. CONCLUSION

This study investigated how reservoir and well parameters influence the distributions of dimensionless pressure and its derivative for a horizontal well in an anisotropic reservoir without top and bottom boundaries but with lateral extent. Increasing horizontal well length hastens the sealing boundary effect, so a shorter well length will eventually ensure optimized production. Longer laterals sense the sealing boundary earlier, while shorter laterals prolong productive performance. The reservoir length, irrespective of the extent, ensures a constant rate of production at early times. However, at transitional and late times, large reservoir length reduces the production in that reservoir. Hence, a reservoir with a short length will improve production. The reservoir production will relatively require an enhanced recovery approach sooner since the boundaries are sealing with no natural external drive/pressure support. Production is not affected by reservoir width regardless of the extent at early times. But at late times, shorter reservoir width improves the rate of production compared to a longer width. A good permeability will generally improve the production rate. The time at which the boundary effect is experienced depends largely on vertical permeability, well length, porosity, and the permeability parallel to the well. These findings provide practical guidance for well design and optimal well placement to enable efficient oil withdrawal in vertically boundless reservoirs.

CONFLICT OF INTEREST

No conflict of interest was declared by the authors.

REFERENCES

[1] Agho, E. Q. (2022). Pressure and Pressure derivative of a horizontal well subjected to a single edge and bottom water drive mechanism in an

anisotropic reservoir. *FUPRE Journal of Scientific and Industrial Research, 6*(2), 106-118

[2] Cui, Q., Zhao, Y., Zhang, L., Chen, M., Gao, S., & Chen, Z. (2023). A semi analytical model of fractured horizontal well with hydraulic fracture network in shale gas reservoir for pressure transient analysis. *Advances in Geo Energy Research, 8*(3), 193–205.

[3] Gringarten, A. C. (2008). The Evolution of the State of the Art in Well Test Analysis. *SPE Reservoir Evaluation & Engineering, 11*(1), 41–62.

[4] Gringarten, A. C., & Ramey, H. J., Jr. (1973). The use of source and Green's functions in solving unsteady-flow problems in reservoirs. *SPE Journal, 13*(5), 285–296.

[5] Huang, T., Guo, X., Peng, K., Song, W., & Hu, C. (2022). Modeling the transient flow behavior of multi-stage fractured horizontal wells in the inter-salt shale oil reservoir, considering stress sensitivity. *Processes, 10*(10), 2085. https://doi.org/10.3390/pr10102085

[6] Idudje, E. H., & Adewole, E. S. (2020). A new test analysis procedure for pressure drawdown test of a horizontal well in an infinite-acting reservoir. *Nigerian Journal of Technology, 39*(3), 816-820.

[7] Liu, C. Q., Yang, Z. B., Chen, H. Q., et al. (2025). A semi-analytical model for flow regime diagnosis in multi-fractured horizontal wells within deep coalbed methane reservoirs. *Journal of Petroleum Exploration and Production Technology, 15*, Article 97. https://doi.org/10.1007/s13202-024-01797-3

[8] Odeh, A. S., & Babu, D. K. (1989). Productivity of a Horizontal Well. *SPE Reservoir Engineering, 4*(4), 417–421.

[9] Olokor, W. F., & Adewole, E. S. (2024). [Title related to horizontal well test interpretation]. *Journal of Engineering for Development, 16*(2), 110–129.

[10] Orene, J. J., & Adewole, E. S. (2020). Pressure distribution of a horizontal well in a bounded reservoir with constant pressure top and bottom. *Nigerian Journal of Technology, 39*(1), 154–160.

[11] Wang, H., Liu, T., Sun, Z., Wang, C., Zhang, Y., Chen, Y., Liu, Z., & Zhou, Z. (2023). Pressure transient analysis of multistage fractured horizontal wells based on detailed characterization of stimulated area. *Frontiers in Energy Research, 10*, Article 987098. https://doi.org/10.3389/fenrg.2022.987098

[12] Zhao, Z., Li, Y., Jiang, T., Hu, D., Zhang, L., & Ma, R. (2022). Analysis and application of horizontal well test in low-permeability porous carbonate reservoir. *Processes, 10*(8), Article 1545. https://doi.org/10.3390/pr10081545

NOMENCLATURE

$h_D = \frac{2h}{L}\sqrt{\frac{k}{k_z}}$, $z_D = \frac{2z}{L}\sqrt{\frac{k}{k_z}}$, $y_D = \frac{2y}{L}\sqrt{\frac{k}{k_y}}$, $L_D = \frac{L}{2h}\sqrt{\frac{k_z}{k}}$,

$x_{wD} = \frac{2x_w}{L}\sqrt{\frac{k}{k_x}}$, $z_{wD} = \frac{2z_w}{L}\sqrt{\frac{k}{k_z}}$, $x_{eD} = \frac{2x_e}{L}\sqrt{\frac{k}{k_x}}$, $y_{eD} = \frac{2y_e}{L}\sqrt{\frac{k}{k_y}}$,

$z_{eD} = \frac{2z_e}{L}\sqrt{\frac{k}{k_z}}$, $x_D = \frac{2x}{L}\sqrt{\frac{k}{k_x}}$, $h_D = \frac{2h}{L}\sqrt{\frac{k}{k_z}}$, $y_{wD} = \frac{2y_w}{L}\sqrt{\frac{k}{k_y}}$,

$r_{wD} = \frac{2r_w}{L}\left(\sqrt{\frac{k}{k_y}} + \sqrt{\frac{k_x}{k}}\right)$,

h_D: Reservoir height (pay thickness),

k_x: Permeability in the x-direction,

k_y: Permeability in the y-direction,

k_z: Permeability in the z-direction,

L: Horizontal well length,

xD: Perforation length,

xe: Reservoir length,

ye: Reservoir width,

L_D: Dimensionless well length,

x_{eD}: Dimensionless reservoir length,

y_{eD}: Dimensionless reservoir width,

r_{wD}: Dimensionless well radius,

z_{wD}: Vertical stand-off ratio,

p_D: Dimensionless pressure,

p'_D: Dimensionless pressure derivative,

t_D: Dimensionless time,

n: Number of image wells,

ze: Vertical distance between drain hole no-flow boundaries,
zw: Vertical distance from the wellbore to the bottom boundary (stand-off).